# Non-autonomy of age-related morphological changes in the *C. elegans* germline stem cell niche

*Running title: aging niche morphology*

Nilay Gupta[1,2]
Mia Sinks[2]
E. Jane Albert Hubbard[2,3]

[1] Department Biology, New York University
[2] Department of Cell Biology, NYU Grossman School of Medicine
[3] Corresponding author jane.hubbard@nyulangone.org

Keywords: aging, stem cell, DAF-16/FOXO, Insulin/IGF-like signaling (IIS), distal tip cell (DTC)

## ABSTRACT

A decline in tissue renewal and repair due to changes in tissue stem cells is a hallmark of aging. Many stem cell pools are maintained by interaction with morphologically complex local niches. Using the *C. elegans* hermaphrodite germline stem cell system, we analyzed age-related changes in the morphology of the niche, the distal tip cell (DTC), and identified a molecular mechanism that promotes a subset of these changes. We found that a long-lived *daf-2* mutant exhibits a *daf-16*-dependent decline in number and length of long DTC processes. Surprisingly, the tissue requirement for *daf-16(+)* is non-autonomous and is independent of the longevity requirement: *daf-16(+)* in body wall muscle is both necessary and sufficient. We also determined that pre-formed DTC processes deteriorate prematurely when the underlying germline differentiates. We propose a reciprocal DTC-germline interaction model and speculate a mechanism by which reducing *daf-2* activity prevents stem cell exhaustion. These studies establish the *C. elegans* DTC as a powerful *in vivo* model for understanding age-related changes in cellular morphology and their consequences in stem cell systems.



## SUMMARY

The *C. elegans* germline stem cell niche morphology is markedly altered with age and is regulated non-autonomously from the muscle by insulin/IGF-like signaling. Results suggest reciprocal niche-germline regulation.

## INTRODUCTION

Age-related changes in cell morphology can alter cell-cell interactions and signaling (Lopez-Otin et al., 2023). Such changes are particularly important to understand in stem cell systems where niche cells can take on complex morphologies and associate intimately with the stem cells they regulate (Brunet et al., 2023). Age-related changes in the cytoskeleton, extracellular matrix, cell adhesion properties, and other factors influence cell morphology and function (DiLoreto and Murphy, 2015).

Here, we investigate age-related morphological changes in a simple stem cell niche *in vivo*. Like many mammalian stem cell systems (Brunet et al., 2023; Lopez-Otin et al., 2023), the *C. elegans* hermaphrodite germline stem cell pool becomes depleted with age (Garigan et al., 2002; Killian and Hubbard, 2005; Kocsisova et al., 2019; Luo et al., 2010; Qin and Hubbard, 2015). The niche in this system is a single cell, the distal tip cell (DTC), that caps the end of the gonad (Fig. 1) and produces membrane-bound DSL family ligands, APX-1 and LAG-2, that activate Notch pathway signaling in juxtaposed germline stem cells (Austin and Kimble, 1987; Henderson et al., 1994; Kimble and White, 1981; Nadarajan et al., 2009). The adult DTC morphology is complex, with variable numbers and lengths of long cytoplasmic processes that extend over and between germline stem and progenitor cells (Byrd et al., 2014; Hall et al., 1999; Tolkin et al., 2024). DTC processes are not essential for establishment of the stem cell pool that occurs during larval stages, but they contribute to contact-dependent Notch signaling in adults (Lee et al., 2016).

Here we present an aging time-course analysis of changes in DTC morphology and identify molecular mechanisms that delay or hasten them. Our analysis reveals several striking changes to DTC morphology with age. We confirm an age-related proximal shift in nuclear position that occurs at high penetrance (as seen by others under different life history and age conditions (Kocsisova et al., 2019; Urman et al., 2024)), and that the number and length of long continuous DTC processes decline with age. We examined these phenotypes for their dependence on the DAF-2 insulin-like signaling (IIS) pathway, which influences lifespan. IIS had a relatively minor effect on the nuclear position, but the effects of age on DTC process number and length were highly IIS-dependent. In the *daf-2* mutant, long DTC processes persist with age, and this persistence requires DAF-16/FOXO. Surprisingly, the cellular requirement for *daf-16* is neither the DTC itself, nor the intestine where it is implicated in longevity. Instead, *daf-16(+)* activity in the body wall muscle is both necessary and sufficient to regulate age-related changes to the length of the DTC processes. We also determined that pre-formed DTC

processes deteriorate prematurely when the underlying germline ceases cell division by differentiating. We propose a reciprocal DTC-germline interaction feedback model whereby a slow germ cell division cycle in *daf-2* mutants delays stem cell exhaustion, in part, by stabilizing DTC processes which then signal to germline stem cells.

## RESULTS

### *Adult DTC morphology is altered with age*

Age-related changes to hermaphrodite DTC features have been reported previously on a short aging timeline and/or in mated worms (to 5 days of adulthood). These include a proximally displaced nucleus (Kocsisova et al., 2019; Urman et al., 2024) and an increase in the size, though not number, of gaps seen using a membrane reporter (Urman et al., 2024). We sought to further characterize changes to DTC morphology in intact live self-fertile worms over a more extensive timeline from Day 1 to Day 10 of adulthood, and to define morphometric parameters to describe and compare age-related changes under different genetic conditions.

To analyze DTC morphology over time, we selected three time points starting from the mid-L4 as determined by vulval morphology (Mok et al., 2015): Day 1 (24 hours post mid-L4), when DTC elaboration has peaked in the wild type; Day 6 post mid-L4, when the reproductive phase of wild-type self-fertile hermaphrodites is ending; and Day 10 post mid-L4, when worms are on the verge of the steep population decline consistent with their ~2-3 week lifespan. To minimize variability due to subtle differences in rearing conditions, for each cohort analyzed, worms were picked as mid-L4 larvae on the same day and harvested for live imaging on Days 1, 6, and 10.

We examined several different transgenes expressing fluorescent proteins in the DTC, settling on *qIs57* which encodes GFP under the control of the *lag-2* promoter (Siegfried et al., 2004). Compared to the other transgenes we examined, it revealed a suitably detailed set of morphological features, did not appreciably dim with age, and allowed tracking of the position of the nucleus (Fig. S1). To ensure that the transgene was not itself modulating lifespan, we performed lifespan analyses in parallel with the canonical wild-type strain N2 and found no significant difference (Fig. 1A). However, a greater percentage of worms were censored in strains bearing *qIs57* (see Materials and methods). Adult DTCs are morphologically variable; two DTCs from each timepoint are shown in Figure 1B and additional examples are in Figure S2.

111 Using our image analysis pipeline (Gupta et al., 2024), we found several striking
112 changes to DTC morphology with age. Day 1 to Day 10 provides the most informative
113 comparisons (Fig. 1B,C; see Fig. S3 for additional timepoints). First, recapitulating and
114 extending the findings of others (Kocsisova et al., 2019; Urman et al., 2024), we observed that
115 the DTC nucleus, which normally sits at the distal end of the DTC, shifts proximally with age.
116 The percentage of DTCs with the nucleus ≥5 μm from the distal end went from 13% at Day 1 to
117 77% at Day 10, and these nuclei averaged 3 μm and 9 μm from the distal end at Day 1 and Day
118 10, respectively. Second, the number and length of processes extending proximally from the
119 DTC (Byrd et al., 2014; Hall et al., 1999; Tolkin et al., 2024) provided additional parameters. We
120 focused on those DTC processes that appeared continuous with the cell body in maximum
121 projection micrographs ("continuous processes" (CPs); Gupta et al., 2024; Tolkin et al., 2024).
122 Our methods do not distinguish between previously-defined subclasses of DTC processes that
123 intercalate with or extend along the germ cells (Byrd et al., 2014), but they reflect only gross
124 morphological features including the proportion of DTCs with processes that extend beyond a
125 20 μm threshold from the distal end, and the numbers and lengths (mean and maximum) of
126 such processes. At Day 1 post mid-L4, all DTCs had at least one process extending beyond 20
127 μm. By Day 10, 14% of DTCs had no CPs beyond this threshold. Among those DTCs with one
128 or more CP over the threshold, we observed fewer and shorter CPs over time: the mean
129 number of CPs decreased from 11 to 4 from Day 1 and Day 10, as did their mean and
130 maximum lengths (mean 37 to 30 μm, and maximum 60 to 38 μm) (Fig. 1C).
131

132 ***Insulin/insulin-like growth factor-1 signaling (IIS) promotes age-related changes in DTC***
133 ***process number and length***

134 The IIS pathway is highly conserved and modulates longevity in *C. elegans*, *Drosophila*,
135 and mice (Kenyon, 2010b; Murphy and Hu, 2013; Russell and Kahn, 2007). In addition to
136 longevity, IIS regulates various physiological processes in *C. elegans*, including development,
137 metabolism, and stress resistance (Murphy and Hu, 2013). DAF-2 is the sole insulin/IGF-1
138 receptor in *C. elegans* (Kimura et al., 1997), and reducing *daf-2* activity (e.g. by the reduction-of-
139 function *(rf) daf-2(e1370)* allele) extends lifespan (Kenyon et al., 1993). To determine whether a
140 reduction in *daf-2* activity would affect age-related changes in DTC morphology, we examined
141 DTCs in *daf-2(rf)* worms. First, we tested whether the *qIs57* marker affected the *daf-2(rf)*
142 longevity phenotype and found that, if anything, the percentage of worms alive between 40-60
143 days was elevated, but the maximum lifespan was similar (Fig. 1A). We aged cohorts of wild-
144 type and *daf-2(rf)* worms in parallel and measured the parameters as described above.

First, we found that *daf-2(rf)* had a minimal and variable effect on age-related nuclear position displacement (Figs 1C, S3). Relative to the wild type, *daf-2(rf)* displayed a reduced proportion of DTCs that exhibit nuclear displacement of ≥5 μm at Day 10. However, a large percentage (47%) of *daf-2(rf)* worms nevertheless displayed the nuclear displacement phenotype (versus 77% in the wild type), and the average degree of displacement in microns from the distal end was similar to the wild type in this cohort. The latter finding is consistent with those of Kocsisova et al. (Kocsisova et al., 2022 Fig. S1). In summary, nuclear displacement occurs at a high penetrance in both wild type and *daf-2(rf)* with an equal distance of displacement, suggesting that IIS plays a minor role in regulating this aspect of age-related changes to DTC morphology.

In contrast to the minor effects on nuclear position, reducing *daf-2* activity virtually halted age-related changes in CP number and length from Day 1 to Day 10: all *daf-2(rf)* worms possessed at least one CP ≥20 μm at Day 10, and there was no decrease in the average number of CPs ≥20 μm, nor their mean or maximum lengths, as was seen in the wild type (Figs 1C, S4). We therefore focused on the DTC phenotypes related to number and length of CPs.

***The persistence of DTC process number and length in daf-2(rf) does not correlate temporally with extended lifespan or reproductive span***

In addition to lifespan extension in *daf-2(rf)*, the reproductive span of self-fertile hermaphrodites averages several days longer (Dillin et al., 2002), and in mated hermaphrodites, the *e1370* allele, in particular, delays reproductive aging (Kocsisova et al., 2022). We wondered whether the rate of age-related changes in the number and length of DTC processes might correlate with reproductive span and/or population lifespan. If correlated with reproductive span, we would expect DTC processes to be shorter after an additional week in *daf-2(rf)*. If the rate of decline were associated with average lifespan, we would expect to observe shorter processes by 30 days. We therefore collected additional measurements in *daf-2(rf)* up to Day 30 (Fig. 1D; additional timepoints in Fig. S3B). Referencing our lifespan measurements, Day 30 in *daf-2(rf)* reflects the percent alive of wild type at Day 15. We found that, remarkably, while the number of CPs declined modestly in this cohort by Day 30 (Fig. 1D), it still remained above that of the wild type at Day 10 (Fig. 1C). In addition, there was no statistically significant decline in the mean length of CPs ≥20 μm up to 30 days, and only a modest decline in the maximum length.

We conclude that reducing *daf-2* markedly delays age-related changes in the number and length of long DTC processes, and that these changes in DTC morphology do not directly correlate with temporal extension of reproductive span or of population lifespan.

179

180 ***Insulin/insulin-like growth factor-1 signaling (IIS) acts via DAF-16/FOXO to promote age-***
181 ***related changes in DTC process length***

182 Many phenotypes of *daf-2(rf)* mutants, including age-related phenotypes such as
183 lifespan, depend on the DAF-16/FOXO transcription factor (Kenyon, 2010a; Murphy and Hu,
184 2013).To determine whether the *daf-2*-dependent age-related changes in DTC process number
185 and length are also dependent on *daf-16*, we examined DTC morphology, as visualized with the
186 *qIs57* marker, in double mutant strains bearing a *daf-16* null mutation *daf-16(mu86)* and *daf-*
187 *2(e1370)* [hereafter referred to as *daf-16(0); daf-2(rf)*]. Although the vast majority of DTCs had
188 one or more CP that exceeded 20 µm, the number of processes and their mean and maximum
189 length decreased similar to the wild type (Fig. 2).

190 To assess the loss of *daf-16* alone, we measured the same parameters in parallel
191 cohorts with the wild type, *daf-2(rf)*, and *daf-16(0); daf-2(rf)* (Figs 2, S5). In these trials, a small
192 but significant percentage of CPs of Day 10 DTCs in *daf-16(0)* worms did not exceed 20 µm,
193 though not as many as the wild type. CP number and length also decreased, as in the wild type.
194 Taken together, we conclude that the maintenance of DTC process number and length over
195 time in *daf-2(rf)* is highly dependent on *daf-16* activity.

196

197 ***Non-autonomous daf-16 activity influences age-related decline of DTC process length***

198 Prior studies indicated that *daf-16* activity in specific tissues can influence distinct
199 phenotypes while also contributing to systemic effects. For example, intestinal *daf-16* is
200 associated with enhanced stress resistance and increased longevity (Libina et al., 2003; Zhang
201 et al., 2022), and *daf-16* in the germ line and muscle promotes expansion of the progenitor pool
202 during germline development (Michaelson et al., 2010). Additionally, *daf-16* activity in *fos-1a*
203 expressing cells in the proximal somatic gonad (PSG) prevents the age-dependent decline in
204 number of germline progenitors (Qin and Hubbard, 2015). Therefore, we sought to determine in
205 which tissues *daf-16* most influences the maintenance of DTC processes with age that we
206 observed in *daf-2(rf)*. For this analysis, we focused on the DTC length parameters (mean and
207 maximum).

208 Our first approach took advantage of available extrachromosomal arrays (Libina et al.,
209 2003; Qin and Hubbard, 2015). Each includes a tissue-restricted promoter driving a GFP::DAF-
210 16a translational fusion. We performed the aging time course in the *daf-16(0); daf-2(rf)*
211 background and compared DTC processes length parameters from control and array-bearing
212 (phenotypically Rol) worms, and non-array bearing (phenotypically non-Rol) progeny from the

213 same array-bearing mothers. If *daf-16(+)* activity were important in a particular tissue location,
214 we expected that its expression would preserve DTC process length relative to *daf-16(0); daf-*
215 *2(rf)*.
216 To assess the approach, we first examined CPs in worms bearing an array that
217 expresses *daf-16a* from the *daf-16* promoter. We observed that all parameters (the proportion of
218 worms with DTC CPs over 20 μm, and the CP number and length – both mean and maximum)
219 were markedly stable relative to *daf-16(0); daf-2(rf)* (Fig. 3) and to non-array bearing siblings
220 (Fig. S6). The phenotypic similarity of *daf-16(0); daf-2(rf)* to non-array bearing progeny from
221 array-bearing mothers also suggested that the array did not confer a maternal effect.
222 We next tested for DTC-autonomy, expressing *daf-16a* from the *lag-2* promoter
223 (Michaelson et al., 2010). Surprisingly, ~15% of ~140 DTCs exhibited an unusual morphology at
224 Days 6 and 10, half displaying uncharacteristically long DTC processes, while others displayed
225 one thick CP containing a displaced nucleus (Fig. S7). None of these features were observed
226 under any other condition. Among the remaining ~85% of DTCs that exhibited normal
227 morphology, the CP length parameters were similar to *daf-16(0); daf-2(rf),* even though ~10% of
228 the DTCs in array-bearing worms at Day 10 had no CPs ≥ 20 μm (Fig. 3, S6). Thus, apart from
229 the low-penetrance alterations in gross morphology, *lag-2*-driven *daf-16a(+)* had no appreciable
230 effect on the persistence of DTC process length with age. We conclude that non-autonomous
231 *daf-16a(+)* activity is sufficient to prevent the age-related decline in DTC length when *daf-2* is
232 reduced.
233
234 ***Intestinal activity of daf-16a does not promote age-related DTC length in daf-2(rf)***
235 Both heterologous expression approaches (Libina et al., 2003) and protein degradation
236 approaches (Zhang et al., 2022) indicate that the intestine is the major contributor of *daf-16*
237 activity that confers extended lifespan in *daf-2(rf)*. We speculated that changes in DTC
238 morphology might be a function of overall organismal aging. If so, we would expect that
239 intestinal *daf-16(+)* in the *daf-16(0); daf-2(rf)* mutant background would stabilize DTC
240 processes, similar to *daf-16(+)* driven by its own promoter.
241 Again, using an available transgene expressing *daf-16(+)* that alters lifespan (Libina et
242 al., 2003), we tested the sufficiency of *daf-16a* expressed from an intestine-specific promoter.
243 We found that although all worms bore DTCs with CPs ≥ 20 μm, CP lengths still declined
244 significantly with age, comparable to that observed in *daf-16(0); daf-2(rf)* controls (Fig. 3, S6). In
245 conclusion, although intestinal *daf-16(+)* contributes the majority of the longevity phenotype in

246 *daf-2(rf)* (Libina et al., 2003; Zhang et al., 2022), it does not regulate the length of DTC
247 processes with age.
248
249 **Neuronal *daf-16a(+)* activity mildly influences the age-related changes in DTC length**
250 Although the intestine is the major contributor of *daf-16* on lifespan, there is neuronal
251 contribution as well (Uno et al., 2021; Zhang et al., 2022). We tested an array expressing *daf-*
252 *16a(+)* from a pan-neuronal promoter and observed that while all DTCs in the worms bearing
253 the neuronally-expressed *daf-16a(+)* array contained CPs that crossed the 20 μm threshold, the
254 CPs showed a modest but significant length decline with age. We conclude that neuronal
255 activity of *daf-16(+)* makes a minor contribution to maintaining the length of DTC processes with
256 age in *daf-2(rf)*.
257
258 **Proximal somatic gonad (PSG) *daf-16a(+)* activity does not prevent the age-related loss**
259 **of DTC process length**
260 Previous results indicate that *daf-16a* expressed in *fos-1a*-positive cells of the proximal
261 somatic gonad (PSG) in a *daf-16(0); daf-2(rf)* double mutant delays age-dependent loss of
262 germline progenitors (Qin and Hubbard, 2015), and *daf-16*-dependent DOS-3, a non-canonical
263 ligand for the GLP-1/Notch receptor, was identified as a relevant PSG signal (Zhang et al.,
264 2024). We hypothesized that a PSG signal might also contribute to DTC morphology. Although
265 prior experiments used *naEx239[*pGC629*(fos1p::gfp::daf-16a)* + pRF4*]* in *daf-16(m26); daf-*
266 *2(e1370)* (Qin and Hubbard, 2015), to keep the *daf-16* background consistent, we moved the
267 array into the *daf-16(mu86); daf-2(rf)* background, and measured CP number and length.
268 In short, *daf-16a(+)* activity in the PSG did not prevent the age-dependent loss of DTC
269 process length. However, these worms were markedly less healthy than other strains bearing
270 *daf-16(+)* arrays: only ~50% of worms survived to Day 4, a defect not observed with other *daf-*
271 *16(+)* arrays. Moreover, nearly a third (29%) of worms bearing the array had no DTC process
272 ≥20 μm. Of those that did, the mean and maximum lengths were lower than the control on Day
273 1 and nevertheless continued to decrease with age (Figs 3A, S6).
274 Collectively, these findings demonstrate that the expression of *daf-16a(+)* via *fos-1a*
275 promoter is insufficient to prevent the age-dependent DTC process decline in a *daf-16(0); daf-*
276 *2(rf)* background. This result raises the possibility that while *daf-16a(+)* in the PSG promotes
277 maintenance of the progenitor pool with age (Qin and Hubbard, 2015; Zhang et al., 2024), it
278 does not delay the decline of DTC process length with age.
279

**Germline *daf-16* exerts a minor effect on DTC process length**

The germ line is the major focus of activity for *daf-16* in modulating expansion of the progenitor zone (PZ) in larval stages (Michaelson et al., 2010), and the development of adult DTC morphology is partially dependent on the germ line (Tolkin et al., 2024). To determine whether germline *daf-16* is required for long continuous DTC processes to persist in *daf-2(rf)*, we used RNAi feeding and the *rrf-1* mutant in which RNAi is less effective in the soma but is retained in the germ line (Kumsta and Hansen, 2012; Sijen et al., 2001). We note that in these experiments (as in Fig. 2) *daf-2(rf)* displays an increase in mean (Fig. 3B) and maximum (Fig. S8) CP length from Day 1 to Day 10. We speculate that this may be related to a delay in the PZ reaching its maximum size in *daf-2(rf)* worms (see Discussion). Reducing *daf-16* by RNAi in *rrf-1(+)* eliminated this increase. In the absence of *rrf-1*, the mean CP length increased in both the L4440 control and with *daf-16(RNAi)*, suggesting that the contribution of *daf-16* from the soma is more relevant for this phenotype. For maximum length, however (Fig. S8), a minor effect of *daf-16(RNAi)* is seen in the absence of *rrf-1*. We conclude that the germline *daf-16* plays a minor role in regulating the length of the longest DTC process in *daf-2(rf)* with age.

**Body wall muscle-specific *daf-16a(+)* is sufficient and necessary for the DTC process length reduction with age in *daf-2(rf)***

We measured DTC parameters in *daf-16(0); daf-2(rf)* worms bearing an array expressing *daf-16a(+)* in body wall muscle (*myo-3p::GFP::daf-16a*; Libina et al., 2003). All the worms carrying the array had CPs ≥20 µm (Fig. 3). Furthermore, CP length was maintained in *daf-16(0); daf-2(rf)* relative to controls without the array, and was similar to worms carrying the *daf-16p::daf-16* array (Figs 3A, S6). Together, these findings indicate that array-borne expression of *daf-16a* in body wall muscle is sufficient to maintain the length of DTC processes with age in *daf-2(rf)*.

To assess the necessity of body wall muscle DAF-16, we used an auxin-mediated degron approach (Zhang et al., 2015). We generated a strain bearing *daf-2(rf),* a *TIR1::mRub*y fusion expressed under the *myo-3* promoter (Sabatella et al., 2021) together with degron-tagged DAF-16::GFP (Zhang et al., 2022), and the DTC marker. Following the red and green fluorescent protein tags, we confirmed the tissue-specific expression of TIR1 and auxin-dependent loss of DAF-16. In all of the vehicle controls (*daf-2(rf)* and with TIR1 or the DAF-16::degron alone), the DTCs in *daf-2(rf)* strains not only maintained but increased in length over the 10 day interval, while mean length of DTC processes in the strain bearing both *myo-3p::TIR1* and the degron-tagged DAF-16 decreased (Figs 3C, S6).

These results suggest that *daf-16* in body wall muscle is a major contributor to the persistence of long DTC processes in *daf-2(rf)* with age.

**Body wall muscle DAF-16a attenuates the rate of germline progenitor zone decline with age**

Prior studies implicated muscle-expressed *daf-16a* activity in a minor but significant role downstream of *daf-2* in promoting larval expansion of the germline progenitor pool (Michaelson et al., 2010), whereas it did not significantly influence the endpoint of the progenitor cell number in aged worms (Qin and Hubbard, 2015).

Our DTC morphology analysis prompted us to re-examine the possibility of a role for *myo-3p::daf-16a(+)* in limiting the PZ pool over an aging time-course in *daf-2(rf)*. We found that the PZ pool started with fewer cells on Day 1, consistent with the results of Michaelson et al. (2010). Relative to controls, *daf-16(0); daf-2(rf)* with *myo-3p::daf-16a(+)* does not affect the terminal PZ cell count, consistent with the results of Qin and Hubbard (2015). However, the presence of the *myo-3p::daf-16a(+)* array does attenuate the rate of decline of the PZ, similar to *daf-2(rf)* (Figs 4A, S9). This result suggests that muscle-produced *daf-16(+)* prevents the loss of both the PZ and DTC processes length over time.

**Germline proliferative status is correlated with stability of DTC processes**

A striking feature of the aged *daf-2(rf)* germ line is the relative stability of the PZ pool compared to the wild type (Fig. 4). In mated worms, *daf-2(rf)* also displays a more proximal border of SYGL-1-positive stem cells and a more constant position of meiotic entry relative to the wild type (Kocsisova et al., 2022). We further observed that the mitotic index did not decline significantly from Day 1 to Day 10 in *daf-2(rf)* (Fig. 4B). These results prompted us to consider the relationship between DTC processes, mitotic progression and stem cell fate.

Out-growth of the DTC processes in early adulthood is dependent on an underlying substrate of the undifferentiated germ cells (Byrd et al., 2014; Tolkin et al., 2024). We therefore wondered whether adult DTC processes, once formed, would be stable in the absence of the underlying PZ in early adulthood. We analyzed the number and length of long DTC processes in worms bearing a temperature sensitive allele of *glp-1/* Notch in which the entire PZ differentiates at the restrictive temperature (Austin and Kimble, 1987). We examined the nuclear morphology of distal germ cells and measured DTC parameters from parallel cohorts of worms that underwent the same temperature-shift regime (Fig. 5A). After 24 hours at the restrictive temperature, although virtually all distal germ cells had entered meiotic prophase, the CP

348 number and length parameters were unaffected. By 48 hours, however, the CP length was
349 reduced relative to the wild type (Fig. 5A-C).
350 We conclude that premature differentiation of the PZ pool causes a premature decline in
351 the complexity of the DTC morphology, but with a time delay between differentiation and the
352 decline of DTC processes. Loss of the stem cells eventually leads to changes in DTC
353 morphology that resemble what is seen in older adults.
354
355 **DISCUSSION**
356
357 Here we define age-related changes in DTC niche morphology and assess their
358 dependence on IIS, a molecular mechanism that affects longevity. We found that an age-related
359 shift in DTC nucleus position is only modestly affected by IIS in self-fertile hermaphrodites, as
360 was previously shown in mated worms (Kocsisova et al., 2022), while the decline in the number
361 and length of long DTC processes is highly dependent on IIS. We identify body wall muscle as a
362 major source of a *daf-16(+)*-dependent activity that can support both the persistence of long
363 DTC processes in a *daf-2(rf)* mutant and the underlying germline progenitor pool. Finally, we
364 determine a dependency relationship between the germ cell proliferative state and maintenance
365 of pre-formed DTC processes.
366
367 **A model for reciprocal feedback interactions between the aging germline and niche**
368 In a seeming paradox, *daf-2(+)* expands the larval germline progenitor zone (PZ) but
369 drives loss of the PZ with age, and both effects are dependent on *daf-16*. In larvae, the germline
370 cell cycle is slower in worms with reduced *daf-2* activity and this is dependent on *daf-16(+)* in
371 the germ line and body wall muscle (Michaelson et al., 2010; Roy et al., 2016). In aged adult
372 worms, a larger PZ pool is maintained with reduced *daf-2* activity (Qin and Hubbard, 2015; Fig.
373 4A). In this case, one *daf-16*-dependent signal, DOS-3, from the proximal somatic gonad likely
374 supports GLP-1/Notch activity in the germ line (Zhang et al., 2024). We found that, in addition,
375 both the PZ pool and long DTC processes are maintained in old *daf-2(rf)* adults in a *daf-16(+)*
376 muscle-autonomous manner. The exact *daf-16*-dependent mechanism – and whether it acts on
377 the directly on the DTC, the germline, or both – awaits further study. We speculate that such a
378 factor could be a *daf-16*-dependent secreted factor – e.g., a mitokine or myokine signaling
379 mechanism, or some other mechanism secondary to the IIS role in muscle function (Herndon et
380 al., 2002; Wang et al., 2019).

381 Regardless of the exact mechanism, these observations suggest a model for interplay
382 between the control of cell fate and cell cycle that may contribute to the dynamics of the
383 germline stem cell system over time with age. Several additional relevant features of the system
384 are noted below.
385 First, stem cell fate and cell cycle rate are independently controlled. The PZ consists of a
386 distal-most SYGL-1(+) germline stem cells (GSCs) that are actively responding to GLP-1/Notch
387 (Kershner et al., 2013), as well as their more proximal SYGL-1(-) progeny that complete a cell
388 division before differentiating (Fox and Schedl, 2015). Reducing *glp-1* activity moves the border
389 of the PZ distally and reduces the number of GSCs but, importantly, does not alter their rate of
390 cell cycle progression (Fox and Schedl, 2015; Michaelson et al., 2010; Roy et al., 2016). By
391 contrast, reducing *daf-2* slows the cell cycle (e.g., lowers M-phase and S-phase indices, a rough
392 proxy) in larvae but does not influence the stem versus non-stem cell fate decision governed by
393 GLP-1/Notch (Michaelson et al., 2010; Roy et al., 2016). Worms with reduced *daf-2* activity
394 therefore reach adulthood with fewer cells PZ cells. This pool declines with age, but at a rate far
395 slower than the wild type (Kocsisova et al., 2022; Qin and Hubbard, 2015; Fig. 4A). Second, as
396 in many mammalian stem cell systems (Brunet et al., 2023), *C. elegans* GSCs become depleted
397 over time (Kocsisova et al., 2019; Qin and Hubbard, 2015), and, importantly, the PZ pool is
398 effectively "used up" over time. This is accelerated in the presence of replete sperm that
399 encourage germline flux (Kocsisova et al., 2019; Qin and Hubbard, 2015). In addition, with age,
400 the mitotic index slows, even in the presence of replete sperm (Kocsisova et al., 2019). Finally,
401 in early adulthood, the outgrowth of DTC processes partially depends on adhesion to underlying
402 dividing germ cells (Tolkin et al., 2024).
403 Taking these observations together, we propose a simple two-component feedback
404 system that supports homeostasis of the progenitor pool in early adulthood, the loss of which
405 contributes to the collapse of both niche morphology and the stem cell pool with age. In this
406 model, the early adult PZ steady state is maintained by a combination of DTC-to-GSC signaling
407 via GLP-1/Notch to designate the stem cell fate in responding germ cells, as well as DAF-2-
408 dependent inputs that promote cell cycle progression and stability of DTC processes. Over time,
409 however, as cells cycle and then leave the PZ through differentiation, the pool is depleted,
410 overlying DTC processes become less stable, and shortened DTC processes further deplete the
411 stem cell pool.
412 In the *daf-2(rf)* scenario, we propose that the persistence of slow-cycling yet
413 undifferentiated germ cells promotes the stability of DTC processes, perhaps by adhesion
414 mechanisms similar to those that act in the early adult (Tolkin et al., 2024). This stability could

415 then support DTC-to-GSC interactions along the DTC processes to promote stem cell fate (Fig.
416 5D). This additional GLP-1/Notch signaling afforded by stable DTC processes may, in turn,
417 support the pool of cells in an undifferentiated, proliferation-competent (though slow-cycling)
418 state. Reducing *daf-2* would thereby delay the age-related declines in both the progenitor pool
419 and niche morphology.

420 Temporally, the decline of the stem cell pool and PZ precedes that of the DTC
421 processes (Figs 1,4). Similarly, when germ cells are forced to differentiate, a time delay occurs
422 before the DTC declines (Fig.5). This suggests that the germline-to-DTC stabilization of the
423 processes is important for the behavior of the system. Our observation that loss of *glp-1* leads to
424 premature collapse of already-formed DTC processes also implicates the germline-to-DTC
425 branch of the feedback to maintain DTC processes.

426 While this model provides a framework for reciprocal signaling between DTC processes
427 and the germ line, additional influences act on the system. For example, the regulation of GLP-
428 1/Notch signaling with age (Kocsisova et al., 2019) is complex: in addition to DOS-3-mediated
429 signaling from the proximal somatic gonad (Zhang et al., 2024), the shift in the position of the
430 DTC also alters the patterning of signaling (Urman et al., 2024), and there may be germline-
431 autonomous aspects of reduced GLP-1/Notch signaling since, at least to Day 4, *sygl-1* RNA
432 levels do not change (Urman et al., 2024). Our model also predicts that the effects of DAF-16
433 from the proximal somatic gonad that act on the germ line should affect the DTC too, since they
434 preserve the PZ. However, we did not observe the predicted stabilization of DTC processes
435 when *daf-16(+)* was expressed in the proximal somatic gonad in *daf-16(0); daf-2(rf)*. Finally,
436 many aspects of the germ cell cycle are unusual, including a highly abbreviated G1,
437 constitutively high levels of cyclin E/CDK2 throughout the cell cycle, and transcriptional
438 regulation of CDK-2 through inhibition of DPL-1 (Fox et al., 2011; Furuta et al., 2018). How such
439 cell cycle features may be modified with age is unresolved.
440

441 **General implications for aging stem cell systems and regenerative medicine**

442 Our analysis suggests an unexpected mechanism whereby “hypertrophic” cell cycle
443 promoting activity of a growth factor may lead to age-related stem cell exhaustion that includes
444 interdependence between the stem cells and the niche. Importantly, our results demonstrate
445 that niche morphology is a key aspect of aging stem cell systems. Non-autonomous control of
446 niche morphology, by adjacent stem cells and/or other tissues, may be important in other stem
447 cell systems as well. Our work further suggests that deeper knowledge of *in vivo* interactions

448 that are influenced by cellular morphology and cell cycle as well as cell-cell signaling, are
449 required to promote stem cell regeneration, especially in aging systems.
450
451
452 **MATERIALS AND METHODS**
453
454 ***Nematode strains and maintenance***
455 The *C. elegans* strains utilized in this study were raised on standard nematode growth media
456 (NGM) agar and *E. coli* OP50 at 20ºC, unless otherwise specified. All strains were derived from
457 Bristol N2 (Brenner, 1974). All strains, including their complete genotypes and sources, are
458 provided in Table S1. The strains generated in this study were obtained through genetic crosses
459 and homozygosity was confirmed by progeny testing – visually for strains bearing fluorescent
460 markers or by DNA sequence analysis based on information in WormBase (Davis et al., 2022).
461 Strains generated for this study are GC1593, GC1607, GC1616, GC1676, GC1682, GC1683,
462 GC1691, GC1692, GC1696, GC1778, GC1817, GC1819, and GC1912.
463
464
465 ***Aging and lifespan assays***
466 Multiple plates of approximately 20 L4 hermaphrodites per plate were prepared, and worms
467 were transferred daily to fresh plates to prevent overcrowding and mixing with their progeny.
468 Worms were collected for imaging or PZ counting at intervals indicated. Controls were run in
469 parallel within each cohort; cohorts share a color in each figure that reports DTC morphometrics
470 or PZ nuclei counts, or mitotic index. Lifespan assays (Fig. 1A) started with 100 worms per
471 genotype. For N2 and CB1370, ~15% were censored due to bagging, desiccating on the petri
472 dish wall, or were otherwise missing. For the two strains that contain *qIs57* (JK2869 and
473 GC1607) the rate of censoring for the same reasons was higher, at 40-50%.
474
475 ***Imaging***
476 With the exception of images of GC1412 in Fig. S1, DTC images were acquired using a Apo
477 60X oil immersion lens on a Nikon W1 spinning disk confocal microscope and subsequently
478 processed, quantified, and analyzed as described in Gupta et al., 2024 (Gupta et al., 2024). The
479 DTC was visualized using the *qIs57* GFP marker, with a 488 nm excitation laser set at ≤10%
480 power. The exposure time was set to 100 ms or 1 frame, the EM Gain Multiplier was set to 50,
481 the conversion gain was set to 1, and the readout mode was set to 'EM Gain 10 MHz at 16-bit'.

482 The images were acquired as Z-stacks at 0.5 µm step size and saved in .nd2 format. The
483 excitation laser used for DAPI was 405 nm at 20-30% power, and for RFP was 561 nm at 20-
484 30% power range.
485
486 ***DAPI staining and progenitor zone (PZ) counts***
487 DAPI staining (using Vectashield from Vector Laboratories™ H-1200-10) was performed as
488 described in Pepper et al., 2003, except that fixation and staining were done in a 9-well glass
489 depression plates (Corning™ 7220-85) to minimize the loss of older worms. Images were
490 acquired using a 60X oil immersion lens on a Nikon W1 spinning disk confocal microscope. The
491 progenitor zone (PZ) is defined as the region before the occurrence of more than one crescent-
492 shaped nucleus within the same transverse section of the gonad (Crittenden et al., 2006; Killian
493 and Hubbard, 2005). After visualizing the entire stack, the PZ region of interest was identified,
494 and the nuclei were counted manually using the multi-point tool in ImageJ™.
495
496 ***Auxin-mediated degradation***
497 For auxin-inducible protein degradation (AID) experiments, 3 mM of Indole-3-acetic acid (IAA,
498 auxin) (Thermo Scientific™ A10556.14) or an equivalent volume of carrier EtOH for controls
499 was added to NGM agar prior to pouring plates. OP50 bacteria were concentrated
500 approximately 2x prior to seeding the auxin-containing plates to compensate for auxin inhibition
501 of bacterial growth (Zhang et al., 2022). Worms were cultured on both the auxin-containing
502 plates and the control plates for multiple generations prior to initiating the aging protocol.
503
504 **Analysis of *glp-1(e2141)***
505 Worms were collected at the mid-L4 stage and cultured at 15°C for 48 hours to allow for DTC
506 elaboration comparable to that seen in Day 1 adults raised at 20°C. A group of worms were
507 separated from the cohort and imaged (T0), while the rest were shifted to 25°C and imaged 24
508 and 48 hours later. Cohorts of worms that were grown under the same conditions were split and
509 analyzed live for DTC features or for cell counts after DAPI staining, as described above.
510
511 **RNAi bacterial feeding**
512 RNAi feeding was carried out as previously described (Timmons et al., 2001) with minor
513 modifications. Single colonies of *E. coli* strain HT115 carrying either an empty vector (L4440) or
514 a vector containing *daf-16* cDNA sequences were obtained from frozen stocks on solid LB
515 plates supplemented with 100 µg/ml ampicillin and 10 µg/ml tetracycline, grown overnight at

516 37°C and used to inoculate liquid LB cultures supplemented with 100 µg/ml ampicillin. Cultures
517 were grown at 37°C with shaking for 6-8 hours and used to seed NGM plates supplemented
518 with 100 µg/ml ampicillin and 0.5% β-lactose. Seeded RNAi plates were kept at room
519 temperature for 24 hours prior to adding worms. Complete penetrance of the *bli-3* Bli phenotype
520 was used as a positive control to confirm the efficacy of RNAi reagents in each experimental
521 replicate. Fresh plates were seeded twice a week over the course of the experiment. L4
522 hermaphrodites were cultured on either L4440- or *daf-16* RNAi-seeded plates for 1 generation
523 prior to starting the aging assays.
524
525 ***Statistics***
526 For lifespan assays, the Mantel-Cox log-rank test was used. Fisher's exact test was used for
527 pair-wise comparisons of proportion plots (DTCs with nuclear displacement ≥5 µm and DTCs
528 with any CPs ≥20 µm). For determining significance between nuclear displacement, number,
529 mean length, and maximum length of CPs ≥20 µm, the number of PZ nuclei, or mitotic index:
530 two-tailed t-test for pairwise comparisons (main figures), and two-tailed t-test with Bonferroni
531 correction for multiple comparisons (supplement). When reporting the mean and maximum CP
532 length, we did not include DTCs that with no CPs >20 µm. All sample numbers (n) are reported
533 in figures.
534
535 **ACKNOWLEDGEMENTS**
536 We thank the CGC, which is funded by NIH Office of Research Infrastructure Programs (P40
537 OD010440), NYU Langone's Microscopy Laboratory (RRID: SCR_017934), especially Michael
538 Cammer; this shared resource is partially supported by the Cancer Center Support Grant
539 P30CA016087, and Anke Kloock, Theadora Tolkin, Julie Manikas and Caroline Goutte for
540 advice and support.
541
542 **FUNDING**
543 NIH R01AG065672
544 NYSTEM DOH 01-C32560GG-3450000
545
546

547

548 **FIGURE LEGENDS**

549

550 **Figure 1. The age-related shift in DTC nuclear position and decline in DTC processes**
551 **number and length have different levels of dependence on *daf-2*.**
552 **(A)** Survival curves for *daf-2(+)* and *daf-2(rf)* worms with and without the *qIs57*[*lag-2p::GFP*]
553 transgene. N2 is the standard wild type, and age is indicated in days post mid-L4 stage.
554 **(B)** Representative micrographs of DTCs in live worms of the indicated genotypes at adult Day
555 1, 6 and 10, post mid-L4. The 20 μm region and the area analyzed for number and length of
556 continuous processes (CPs; see Gupta et al., 2024; Tolkin et al., 2024) are indicated, as is the
557 position of the longest CP. Open arrowheads indicate non-DTC structures. Scale bars are 20
558 μm.
559 **(C)** Quantified age-related DTC features (from top left to bottom right): proportion of DTCs with
560 nuclear displacement ≥5 μm (black bar), position of nuclear displacement (μm) from the distal
561 end, proportion of DTCs with any CPs ≥20 μm (black bar), number of CPs ≥20 μm per DTC,
562 mean and maximum length of CPs ≥20 μm per DTC. N values for proportion plots are the same
563 as for the nuclear displacement superplot (top middle). For all superplots, each dot represents a
564 single DTC (n value shown), colors indicate parallel cohorts distinct from those in other main
565 figures, large circles in color are averages for each cohort, the black dot is the pooled average
566 for all cohorts shown, and black line connects pooled average values, indicating the direction
567 and extent of differences between Day 1 and Day 10. Day 10 n values for mean and maximum
568 CP length are lower since only DTCs with CPs >20 μm were included in these measurements.
569 **(D)** Number, mean and maximum length of CPs in *daf-2(rf)* at indicated ages in days post mid-
570 L4.
571 **For all panels**, *qIs57* carries *lag-2p::GFP* and *daf-2(rf)* is *daf-2(e1370).* See methods for
572 statistics details; comparisons are made between Day 1 and Day 10 within a given genotype; for
573 proportion plots, only $p < 0.05$ are indicated; otherwise, NS is "not significant", or $p \geq 0.05$; * $p <$
574 $0.05$, *** $p < 0.001$.

575

576 **Figure 2. Loss of *daf-16* largely reverses the effects of *daf-2* on CP number and length.**
577 From top to bottom: proportion of DTCs with any CPs ≥20 μm (black bars), number of CPs ≥20
578 μm per DTC, mean and maximum length of CPs ≥20 μm per DTC in the indicated genotypes for
579 worms imaged on Day 1 and Day 10 post mid-L4. N values for proportion plots correspond to
580 the "Number of CPs" superplot to the right; n values for mean and maximum length plots reflect

581 only those DTCs with CPs ≥ 20 μm. For superplots, dots and circles are as described in Figure
582 1; colors indicate cohorts and replicates are distinct from those presented in other main figures.
583 See methods for statistics details; NS is "not significant", * p < 0.05, ** p < 0.01, *** p < 0.001,
584 and blue asterisks indicate a significant increase from Day 1 to Day 10.
585
586
587 **Figure 3. *daf-16(+)* in body wall muscle is sufficient and necessary for *daf-2(rf)***
588 **suppression of age-related changes in DTC process length.**
589 **(A)** Proportion of DTCs with CPs ≥20 μm, and mean length of CPs ≥20 μm per DTC for
590 indicated genotypes at Day 1 and Day 10 post mid-L4. N values for mean length plots reflect
591 only those DTCs with CPs ≥ 20 μm. **(B)** Superplots showing mean length of CPs ≥20 μm in
592 genotypes indicated. *L4440* indicates the empty vector control and *daf-16 RNAi* is the vector
593 carrying *daf-16* cDNA sequences. **(C)** Mean length of CPs ≥20 μm in worms raised on 3mM
594 auxin an in genotypes indicated, where *daf-16::degron* is *hq389[daf-16::GFP::degron]* and
595 *Muscle::TIR1* is *emcSi71[myo-3p::TIR-1::mRuby]*. **For all panels,** *qIs57* carries *lag-2p::GFP*,
596 *daf-16(0)* is *daf-16(mu86),* and *daf-2(rf)* is *daf-2(e1370).* For all superplots, colors indicate
597 cohorts within panels; replicates shown here are distinct from those in other main figures. See
598 methods for statistics details; NS is "not significant", * p < 0.05, ** p < 0.01, *** p < 0.001, and
599 blue asterisks indicate a significant increase.
600
601 **Figure 4. The progenitor zone (PZ) and mitotic index are influenced by *daf-16*.**
602 **(A)** The number of PZ nuclei in (n) gonads in worms of the indicated genotypes at Day 1 and
603 Day 10 post mid-L4. **(B)** The mitotic index (number of mitotic figures over total cells in the PZ)
604 in the indicated genotypes at Day 1 and Day 10 post mid-L4. **For all panels,** *qIs57* carries *lag-*
605 *2p::GFP*, *daf-16(0)* is *daf-16(mu86),* and *daf-2(rf)* is *daf-2(e1370).* For all superplots, colors
606 indicate cohorts within panels. See methods for statistics details; NS is "not significant", * p <
607 0.05, ** p < 0.01, *** p < 0.001.
608
609 **Figure 5. Premature decline of DTC processes upon germline stem cell differentiation.**
610 **(A)** Experimental design and images of DAPI-stained control and *glp-1(e2141)* worms at
611 indicated time points and temperatures. **(B)** Examples of DTC morphology in parallel to those
612 shown in panel **(A). (A, B)** Scale bars are 20 μm. **(C)** Quantification of number and length (mean
613 and maximum) of CPs ≥20 μm in control and *glp-1(e2141)* worms at indicated time points.
614 Colors indicate cohorts within panels. See methods for statistics details; NS is "not significant", *

615 $p < 0.05$, *** $p < 0.001$. **(D)** Cartoon representation of a two-component feedback model for
616 niche-stem cell interaction at early and late ("old") adult stages. Dotted box indicates area of
617 direct DTC-germline interaction that is lost with age. White circles represent undifferentiated
618 germ cells, and grey circles represent differentiated germ cells. See text for details.
619
620

621 **REFERENCES**

622


623 **Austin, J. and Kimble, J.** (1987). glp-1 is required in the germ line for regulation of the decision
624 between mitosis and meiosis in C. elegans. *Cell* **51**, 589-599.
625 **Brenner, S.** (1974). The genetics of Caenorhabditis elegans. *Genetics* **77**, 71-94.
626 **Brunet, A., Goodell, M. A. and Rando, T. A.** (2023). Ageing and rejuvenation of tissue stem
627 cells and their niches. *Nat Rev Mol Cell Biol* **24**, 45-62.
628 **Byrd, D. T., Knobel, K., Affeldt, K., Crittenden, S. L. and Kimble, J.** (2014). A DTC niche
629 plexus surrounds the germline stem cell pool in Caenorhabditis elegans. *PLoS One* **9**,
630 e88372.
631 **Crittenden, S. L., Leonhard, K. A., Byrd, D. T. and Kimble, J.** (2006). Cellular analyses of the
632 mitotic region in the Caenorhabditis elegans adult germ line. *Molecular biology of the cell*
633 **17**, 3051-3061.
634 **Davis, P., Zarowiecki, M., Arnaboldi, V., Becerra, A., Cain, S., Chan, J., Chen, W. J., Cho,**
635 **J., da Veiga Beltrame, E., Diamantakis, S., et al.** (2022). WormBase in 2022-data,
636 processes, and tools for analyzing Caenorhabditis elegans. *Genetics* **220**.
637 **Dillin, A., Crawford, D. K. and Kenyon, C.** (2002). Timing requirements for insulin/IGF-1
638 signaling in C. elegans. *Science* **298**, 830-834.
639 **DiLoreto, R. and Murphy, C. T.** (2015). The cell biology of aging. *Mol Biol Cell* **26**, 4524-4531.
640 **Fox, P. M. and Schedl, T.** (2015). Analysis of Germline Stem Cell Differentiation Following
641 Loss of GLP-1 Notch Activity in Caenorhabditis elegans. *Genetics* **201**, 167-184.
642 **Fox, P. M., Vought, V. E., Hanazawa, M., Lee, M.-H., Maine, E. M. and Schedl, T.** (2011).
643 Cyclin E and CDK-2 regulate proliferative cell fate and cell cycle progression in the C.
644 elegans germline. *Development (Cambridge, England)* **138**, 2223-2234.
645 **Furuta, T., Joo, H. J., Trimmer, K. A., Chen, S. Y. and Arur, S.** (2018). GSK-3 promotes S-
646 phase entry and progression in C. elegans germline stem cells to maintain tissue output.
647 *Development* **145**.
648 **Garigan, D., Hsu, A. L., Fraser, A. G., Kamath, R. S., Ahringer, J. and Kenyon, C.** (2002).
649 Genetic analysis of tissue aging in Caenorhabditis elegans: a role for heat-shock factor
650 and bacterial proliferation. *Genetics* **161**, 1101-1112.
651 **Gupta, N., Cammer, M., Tolkin, T. and Hubbard, E. J. A.** (2024). A DTC morphometrics
652 package for quantification of complex and variable cellular morphology using ImageJ.
653 *MicroPubl Biol* **2024**.
654 **Hall, D. H., Winfrey, V. P., Blaeuer, G., Hoffman, L. H., Furuta, T., Rose, K. L., Hobert, O.**
655 **and Greenstein, D.** (1999). Ultrastructural features of the adult hermaphrodite gonad of
656 Caenorhabditis elegans: relations between the germ line and soma. *Dev Biol* **212**, 101-
657 123.
658 **Henderson, S. T., Gao, D., Lambie, E. J. and Kimble, J.** (1994). lag-2 may encode a signaling
659 ligand for the GLP-1 and LIN-12 receptors of C. elegans. *Development (Cambridge,*
660 *England)* **120**, 2913-2924.
661 **Herndon, L. A., Schmeissner, P. J., Dudaronek, J. M., Brown, P. A., Listner, K. M., Sakano,**
662 **Y., Paupard, M. C., Hall, D. H. and Driscoll, M.** (2002). Stochastic and genetic factors
663 influence tissue-specific decline in ageing C. elegans. *Nature* **419**, 808-814.
664 **Kenyon, C.** (2010a). The first long-lived mutants: discovery of the insulin/IGF-1 pathway for
665 ageing. *Philosophical Transactions of the Royal Society B: Biological Sciences* **366**, 9-
666 16.
667 **Kenyon, C., Chang, J., Gensch, E., Rudner, A. and Tabtiang, R.** (1993). A C. elegans mutant
668 that lives twice as long as wild type. *Nature* **366**, 461-464.
669 **Kenyon, C. J.** (2010b). The genetics of ageing. *Nature* **464**, 504-512.

**Kershner, A., Crittenden, S. L., Friend, K., Sorensen, E. B., Porter, D. F. and Kimble, J.** (2013). Germline Stem Cells and Their Regulation in the Nematode Caenorhabditis elegans. pp. 29-46. Dordrecht: Springer Netherlands.

**Killian, D. J. and Hubbard, E. J. A.** (2005). Caenorhabditis elegans germline patterning requires coordinated development of the somatic gonadal sheath and the germ line. *Developmental Biology* **279**, 322-335.

**Kimble, J. E. and White, J. G.** (1981). On the control of germ cell development in Caenorhabditis elegans. *Dev Biol* **81**, 208-219.

**Kimura, K. D., Tissenbaum, H. A., Liu, Y. and Ruvkun, G.** (1997). daf-2, an insulin receptor-like gene that regulates longevity and diapause in Caenorhabditis elegans. *Science* **277**, 942-946.

**Kocsisova, Z., Bagatelas, E. D., Santiago-Borges, J., Lei, H. C., Egan, B. M., Mosley, M. C., Schneider, D. L., Schedl, T. and Kornfeld, K.** (2022). Notch signaling in germ line stem cells controls reproductive aging in C. elegans. *bioRxiv*.

**Kocsisova, Z., Kornfeld, K. and Schedl, T.** (2019). Rapid population-wide declines in stem cell number and activity during reproductive aging in C. elegans. *Development* **146**.

**Kumsta, C. and Hansen, M.** (2012). C. elegans rrf-1 mutations maintain RNAi efficiency in the soma in addition to the germline. *PLoS One* **7**, e35428.

**Lee, C., Sorensen, E. B., Lynch, T. R. and Kimble, J.** (2016). C. elegans GLP-1/Notch activates transcription in a probability gradient across the germline stem cell pool. *eLife* **5**.

**Libina, N., Berman, J. R. and Kenyon, C.** (2003). Tissue-specific activities of C. elegans DAF-16 in the regulation of lifespan. *Cell* **115**, 489-502.

**Lopez-Otin, C., Blasco, M. A., Partridge, L., Serrano, M. and Kroemer, G.** (2023). Hallmarks of aging: An expanding universe. *Cell* **186**, 243-278.

**Luo, S., Kleemann, G. A., Ashraf, J. M., Shaw, W. M. and Murphy, C. T.** (2010). TGF-β and insulin signaling regulate reproductive aging via oocyte and germline quality maintenance. *Cell* **143**, 299-312.

**Michaelson, D., Korta, D. Z., Capua, Y. and Hubbard, E. J. A.** (2010). Insulin signaling promotes germline proliferation in C. elegans. *Development (Cambridge, England)* **137**, 671-680.

**Mok, D. Z., Sternberg, P. W. and Inoue, T.** (2015). Morphologically defined sub-stages of C. elegans vulval development in the fourth larval stage. *BMC Dev Biol* **15**, 26.

**Murphy, C. T. and Hu, P. J.** (2013). Insulin/insulin-like growth factor signaling in C. elegans. *WormBook*, 1-43.

**Nadarajan, S., Govindan, J. A., McGovern, M., Hubbard, E. J. A. and Greenstein, D.** (2009). MSP and GLP-1/Notch signaling coordinately regulate actomyosin-dependent cytoplasmic streaming and oocyte growth in C. elegans. *Development (Cambridge, England)* **136**, 2223-2234.

**Qin, Z. and Hubbard, E. J. A.** (2015). Non-autonomous DAF-16/FOXO activity antagonizes age-related loss of C. elegans germline stem/progenitor cells. *Nature Communications* **6**, 7107.

**Roy, D., Michaelson, D., Hochman, T., Santella, A., Bao, Z., Goldberg, J. D. and Hubbard, E. J. A.** (2016). Cell cycle features of C. elegans germline stem/progenitor cells vary temporally and spatially. *Dev Biol* **409**, 261-271.

**Russell, S. J. and Kahn, C. R.** (2007). Endocrine regulation of ageing. *Nat Rev Mol Cell Biol* **8**, 681-691.

**Sabatella, M., Thijssen, K. L., Davo-Martinez, C., Vermeulen, W. and Lans, H.** (2021). Tissue-Specific DNA Repair Activity of ERCC-1/XPF-1. *Cell Rep* **34**, 108608.

**Siegfried, K. R., Kidd, A. R., 3rd, Chesney, M. A. and Kimble, J.** (2004). The sys-1 and sys-3 genes cooperate with Wnt signaling to establish the proximal-distal axis of the Caenorhabditis elegans gonad. *Genetics* **166**, 171-186.

**Sijen, T., Fleenor, J., Simmer, F., Thijssen, K. L., Parrish, S., Timmons, L., Plasterk, R. H. and Fire, A.** (2001). On the role of RNA amplification in dsRNA-triggered gene silencing. *Cell* **107**, 465-476.

**Timmons, L., Court, D. L. and Fire, A.** (2001). Ingestion of bacterially expressed dsRNAs can produce specific and potent genetic interference in Caenorhabditis elegans. *Gene* **263**, 103-112.

**Tolkin, T., Burnett, J. and Hubbard, E. J. A.** (2024). A role for organ level dynamics in morphogenesis of the C. elegans hermaphrodite distal tip cell. *Development* **151**.

**Uno, M., Tani, Y., Nono, M., Okabe, E., Kishimoto, S., Takahashi, C., Abe, R., Kurihara, T. and Nishida, E.** (2021). Neuronal DAF-16-to-intestinal DAF-16 communication underlies organismal lifespan extension in C. elegans. *iScience* **24**, 102706.

**Urman, M. A., John, N. S., Jung, T. and Lee, C.** (2024). Aging disrupts spatiotemporal regulation of germline stem cells and niche integrity. *Biol Open* **13**.

**Wang, H., Webster, P., Chen, L. and Fisher, A. L.** (2019). Cell-autonomous and non-autonomous roles of daf-16 in muscle function and mitochondrial capacity in aging C. elegans. *Aging (Albany NY)* **11**, 2295-2311.

**Zhang, L., Ward, J. D., Cheng, Z. and Dernburg, A. F.** (2015). The auxin-inducible degradation (AID) system enables versatile conditional protein depletion in C. elegans. *Development* **142**, 4374-4384.

**Zhang, Y. P., Zhang, W. H., Zhang, P., Li, Q., Sun, Y., Wang, J. W., Zhang, S. O., Cai, T., Zhan, C. and Dong, M. Q.** (2022). Intestine-specific removal of DAF-2 nearly doubles lifespan in Caenorhabditis elegans with little fitness cost. *Nat Commun* **13**, 6339.

**Zhang, Z., Yang, H., Fang, L., Zhao, G., Xiang, J., Zheng, J. C. and Qin, Z.** (2024). DOS-3 mediates cell-non-autonomous DAF-16/FOXO activity in antagonizing age-related loss of C. elegans germline stem/progenitor cells. *Nat Commun* **15**, 4904.

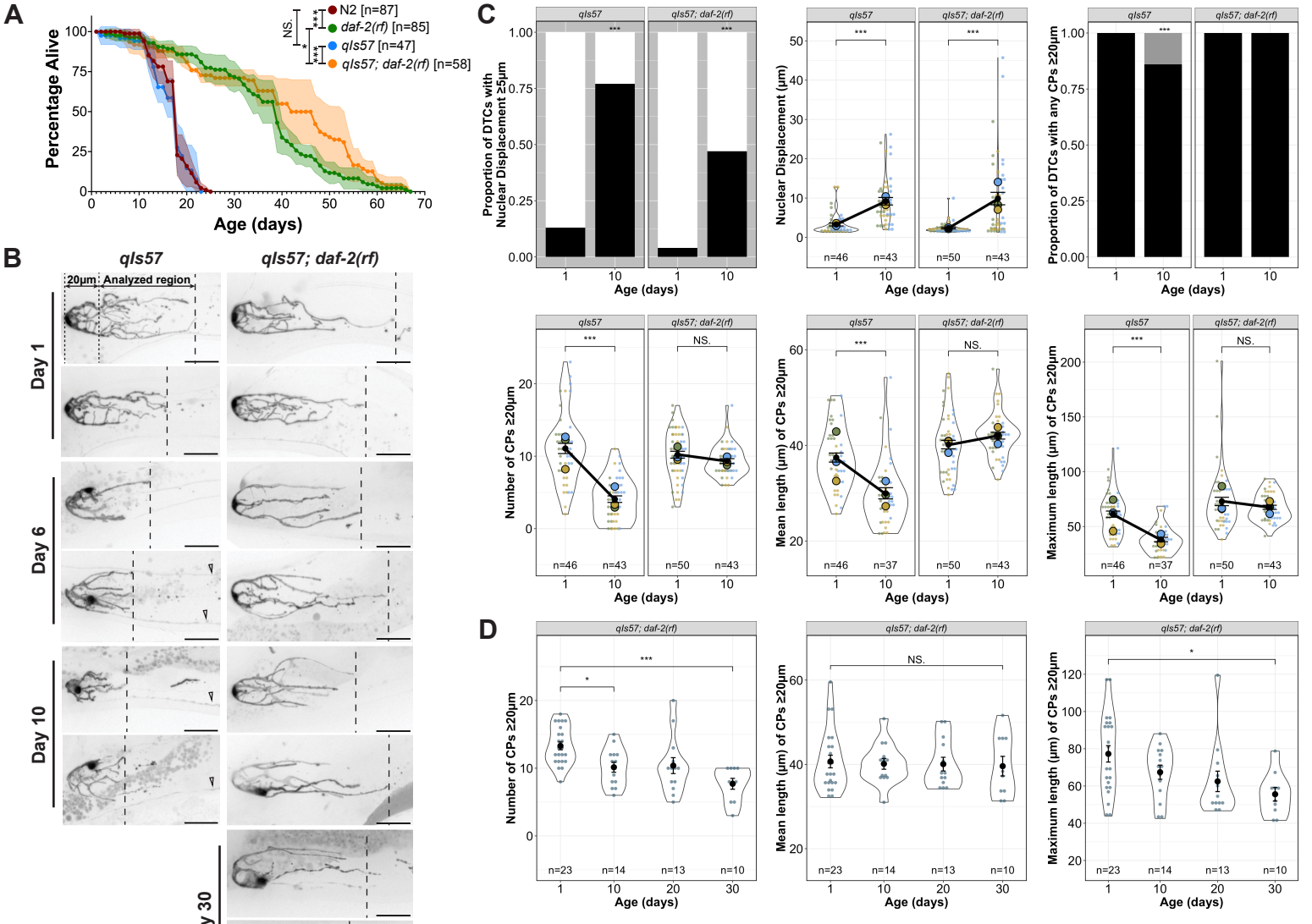
A
N2 [n=87]
daf-2(rf) [n=85]
qls57 [n=47]
qls57; daf-2(rf) [n=58]
Percentage Alive
Age (days)
B
qls57
qls57; daf-2(rf)
20µm
Analyzed region
Day 1
Day 6
Day 10
Day 30
C
qls57
qls57; daf-2(rf)
Proportion of DTCs with Nuclear Displacement ≥5µm
Nuclear Displacement (µm)
Proportion of DTCs with any CPs ≥20µm
Number of CPs ≥20µm
Mean length (µm) of CPs ≥20µm
Maximum length (µm) of CPs ≥20µm
Age (days)
NS.
D
qls57; daf-2(rf)
Number of CPs ≥20µm
Mean length (µm) of CPs ≥20µm
Maximum length (µm) of CPs ≥20µm
Age (days)

**Figure 1**

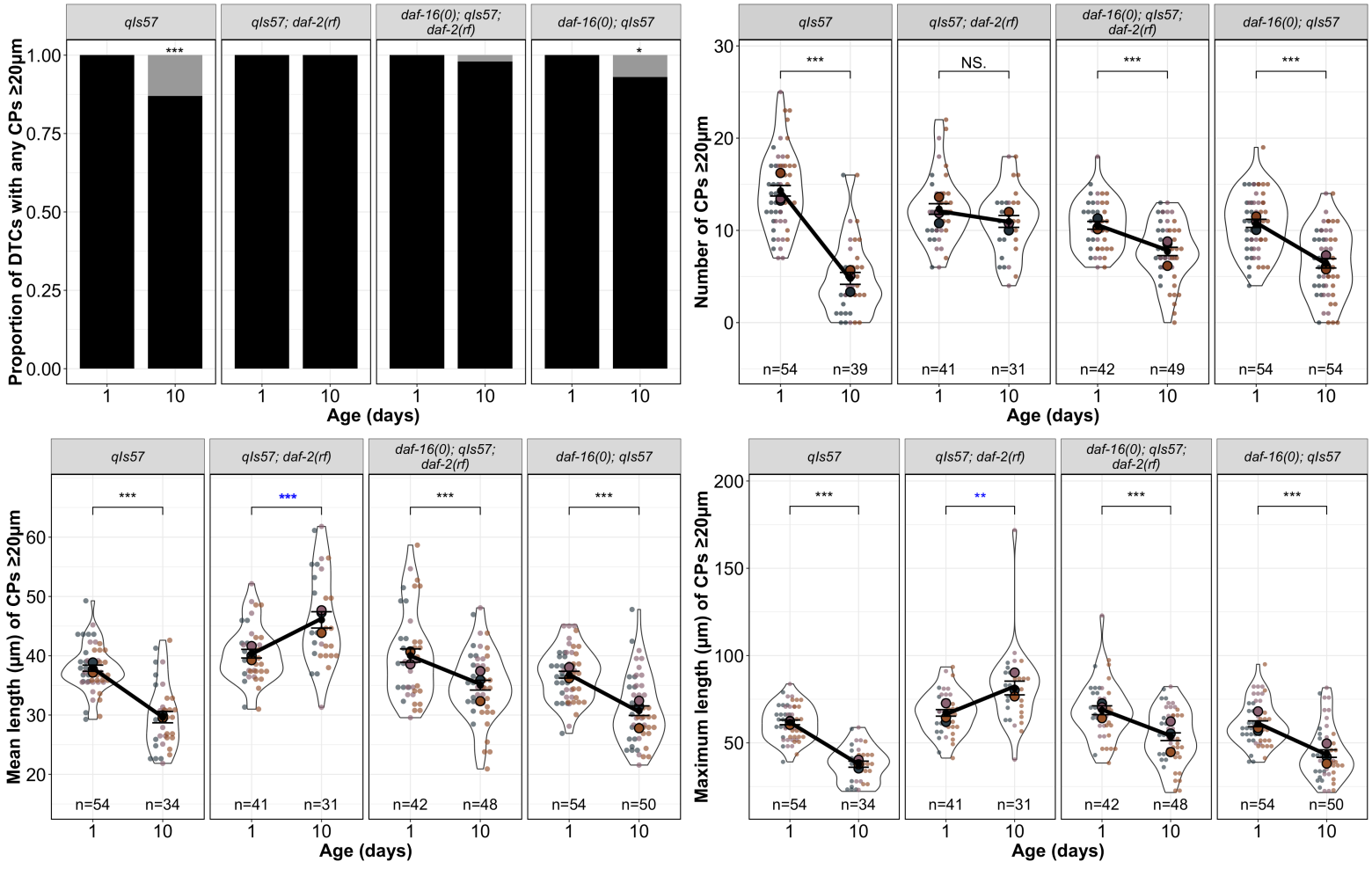
qIs57
qIs57; daf-2(rf)
daf-16(0); qIs57; daf-2(rf)
daf-16(0); qIs57
Proportion of DTCs with any CPs ≥20µm
1.00
0.75
0.50
0.25
0.00
***
*
Number of CPs ≥20µm
30
20
10
0
NS.
n=54
n=39
n=41
n=31
n=42
n=49
n=54
n=54
Mean length (µm) of CPs ≥20µm
60
50
40
30
20
n=54
n=34
n=41
n=31
n=42
n=48
n=54
n=50
Maximum length (µm) of CPs ≥20µm
200
150
100
50
**
1
10
Age (days)

**Figure 2**

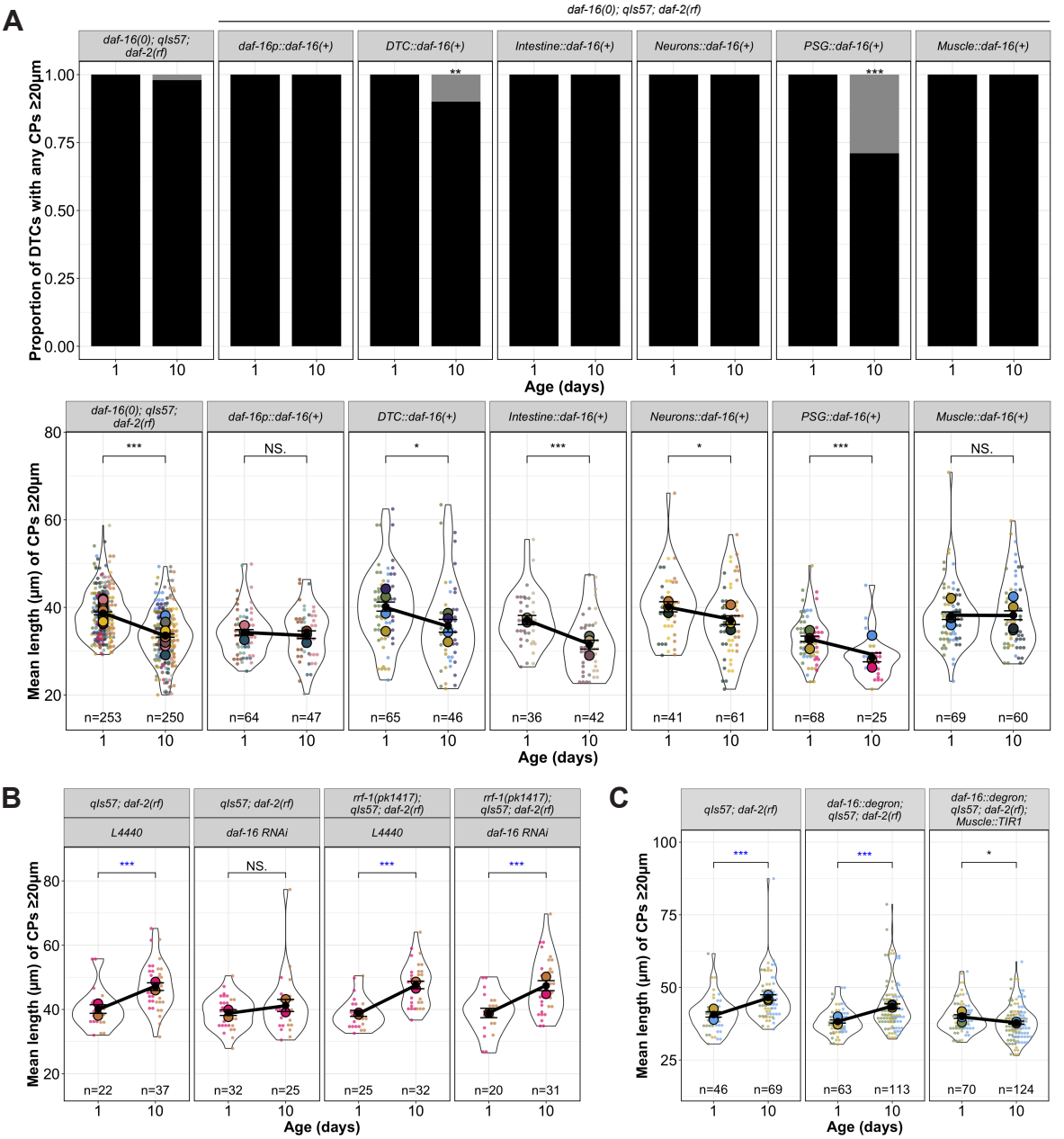
A
daf-16(0); qls57; daf-2(rf)
daf-16(0); qls57; daf-2(rf)
daf-16p::daf-16(+)
DTC::daf-16(+)
Intestine::daf-16(+)
Neurons::daf-16(+)
PSG::daf-16(+)
Muscle::daf-16(+)
Proportion of DTCs with any CPs ≥20µm
1.00
0.75
0.50
0.25
0.00
**
***
1
10
Age (days)
Mean length (µm) of CPs ≥20µm
80
60
40
20
***
NS.
*
n=253
n=250
n=64
n=47
n=65
n=46
n=36
n=42
n=41
n=61
n=68
n=25
n=69
n=60
B
qls57; daf-2(rf)
L4440
qls57; daf-2(rf)
daf-16 RNAi
rrf-1(pk1417); qls57; daf-2(rf)
L4440
rrf-1(pk1417); qls57; daf-2(rf)
daf-16 RNAi
n=22
n=37
n=32
n=25
n=25
n=32
n=20
n=31
C
qls57; daf-2(rf)
daf-16::degron; qls57; daf-2(rf)
daf-16::degron; qls57; daf-2(rf); Muscle::TIR1
100
75
50
25
n=46
n=69
n=63
n=113
n=70
n=124

**Figure 3**

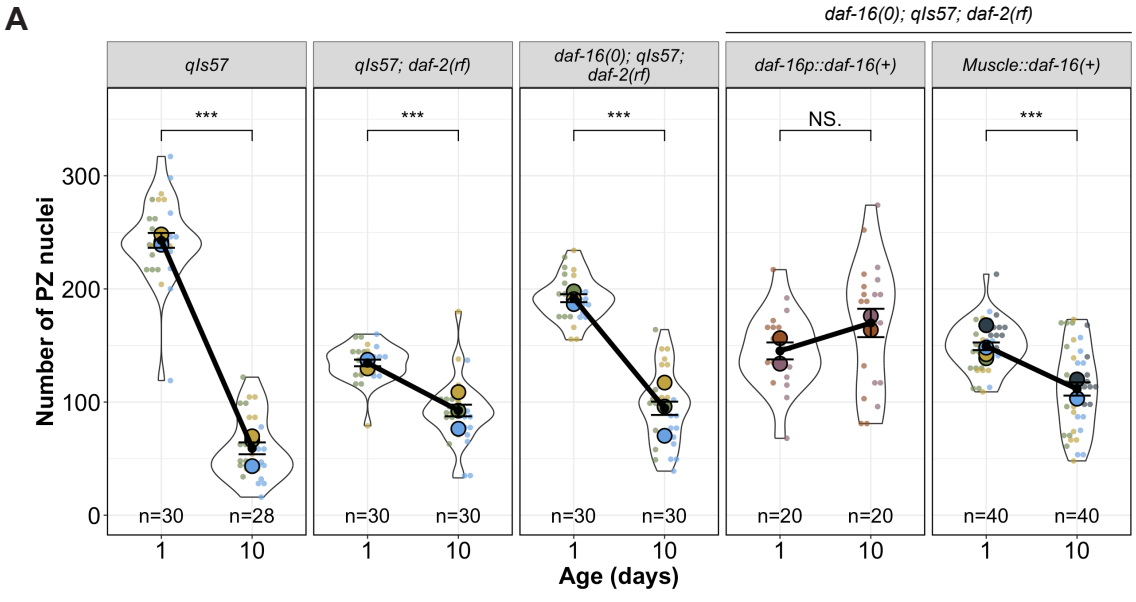
A
daf-16(0); qIs57; daf-2(rf)
qIs57
qIs57; daf-2(rf)
daf-16(0); qIs57; daf-2(rf)
daf-16p::daf-16(+)
Muscle::daf-16(+)
***
***
***
NS.
***
Number of PZ nuclei
300
200
100
0
n=30
n=28
n=30
n=30
n=30
n=30
n=20
n=20
n=40
n=40
1
10
Age (days)

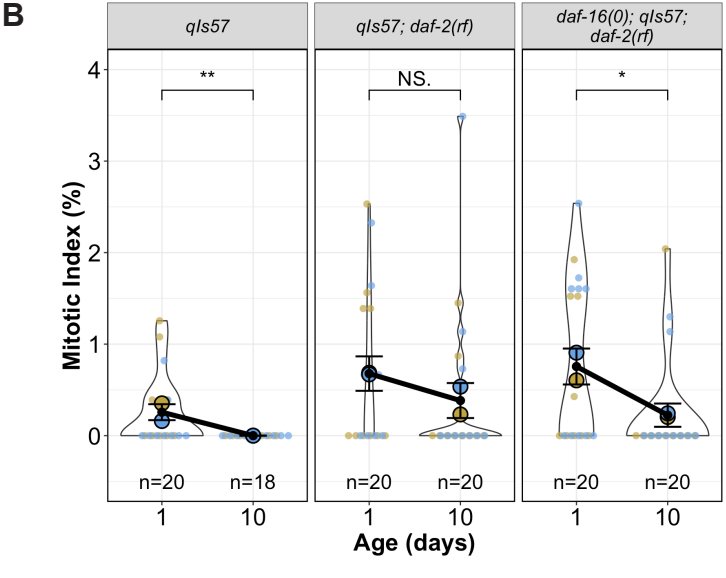
B
qIs57
qIs57; daf-2(rf)
daf-16(0); qIs57; daf-2(rf)
**
NS.
*
Mitotic Index (%)
4
3
2
1
0
n=20
n=18
n=20
n=20
n=20
n=20
1
10
Age (days)

**Figure 4**

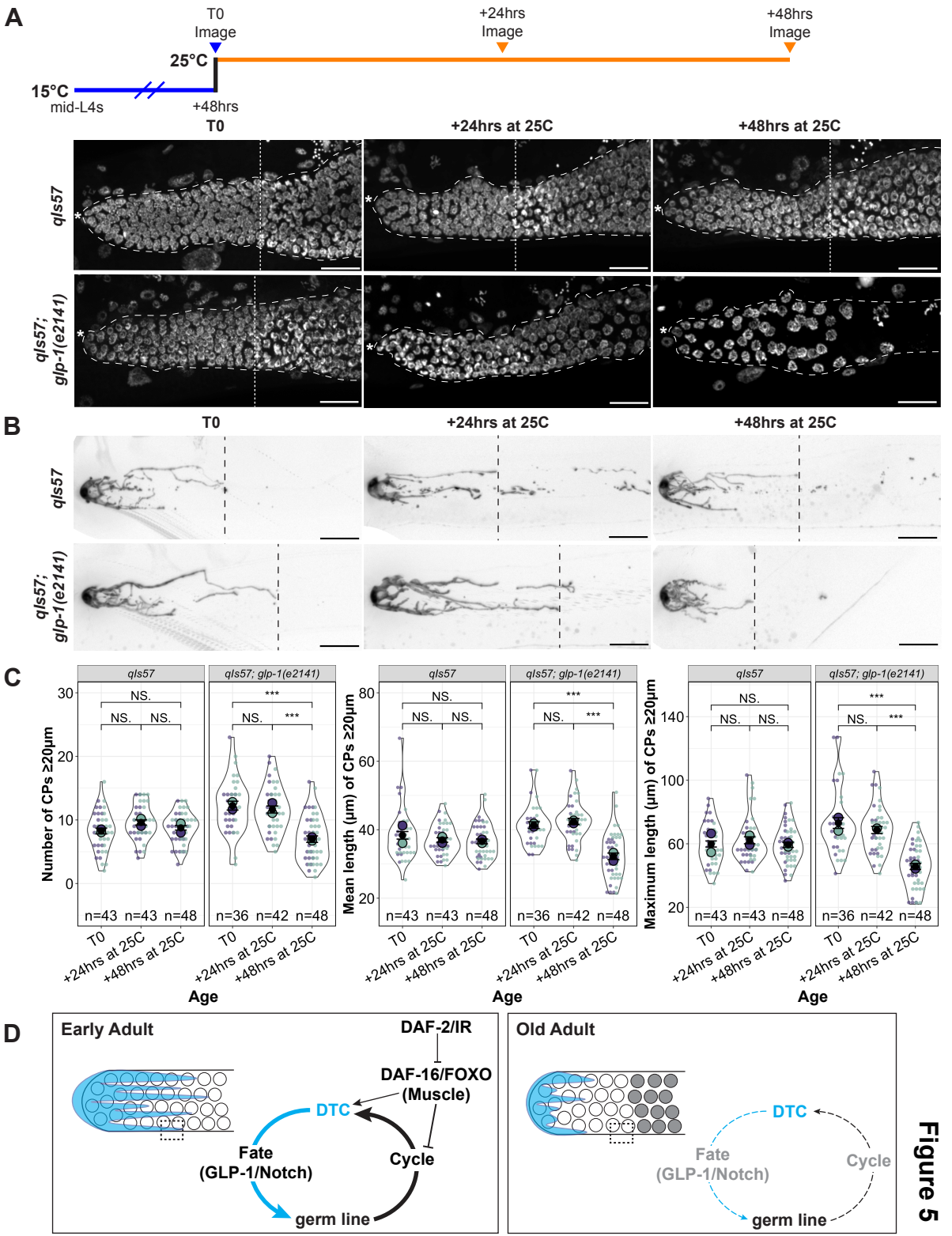
A
T0 Image
+24hrs Image
+48hrs Image
25°C
15°C
mid-L4s
+48hrs
T0
+24hrs at 25C
+48hrs at 25C
qIs57
qIs57; glp-1(e2141)
B
T0
+24hrs at 25C
+48hrs at 25C
qIs57
qIs57; glp-1(e2141)
C
qIs57
qIs57; glp-1(e2141)
Number of CPs ≥20µm
Mean length (µm) of CPs ≥20µm
Maximum length (µm) of CPs ≥20µm
NS.
***
n=43 n=43 n=48
n=36 n=42 n=48
T0
+24hrs at 25C
+48hrs at 25C
Age
D
Early Adult
DAF-2/IR
DAF-16/FOXO
(Muscle)
DTC
Fate
(GLP-1/Notch)
Cycle
germ line
Old Adult
DTC
Fate
(GLP-1/Notch)
Cycle
germ line

Figure 5